MODELLING SEAFLOOR BIOTURBATION

SF Johnson Pennsylvania State University Applied Research Laboratory, State College, PA, USA
DR Jackson University of Washington Applied Physics Laboratory, Seattle, WA, USA

1 INTRODUCTION

The littoral seafloor is a dynamic environment; hydrodynamic and biologic forces continuously modify the seabed relief. Sandy environments are often the most active, with storm and tidal forces organizing sediment into orbital ripples while bottom-feeding and bottom-dwelling organisms rework the seafloor (i.e. bioturbation), destroying this structure and returning it to random equilibrium. Understanding and predicting the temporal evolution of the seafloor is vital for a variety of oceanographic (e.g. hydrodynamic flow in the presence of sand ripples) and acoustic (e.g. synthetic aperture sonar-based coherent change detection) techniques.

In this paper, we present an amalgamation of model and numerical simulation to represent and predict the impact of bioturbation on seabed relief. A previously presented model representative of a fish feeding pit is further developed with consideration of horizontal diffusion, and extended to provide the ability to predict seafloor roughness equilibrium power spectra. This formalization of equilibrium power spectra is compared to numerical simulations for a variety of forcing function sizes and probability density functions.

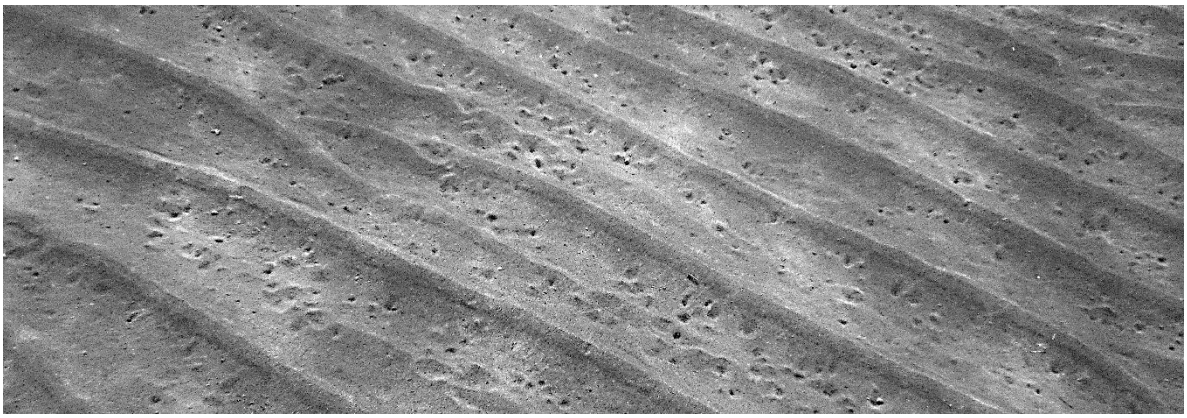

Figure 1: Underwater photograph of near-shore orbital ripples with small fish feeding pits present.

2 AN ANALYTIC MODEL FOR A BIOTURBATIVE EVENT

There are numerous organisms that endlessly interact and rework the seabed by feeding on prey within, burrowing into, or simply moving across the seafloor sediment. Jackson et al.[1] modelled the evolution of seafloor roughness by employing a forcing function determined by fitting observed roughness spectra, without attempting to model individual bioturbative events. Here, specific models for bioturbation will be assumed. The most apparent bioturbative activity observed in recently conducted experiments on sandy seafloors is the reworking of the seabed by fish as they make small pits while feeding (e.g. Figure 1). These feeding pits may be formed when a fish bites a mouthful of sediment containing prey or squirts a jet of water to dislodge the prey. Tang[2] presented a 3-

dimensional version of the 2nd derivative of a Gaussian function (also referred to as (inverted) besinc, jinc, or sombrero functions) as a convenient model for such an "event" (Figure 2). This azimuthally symmetric model can be described analytically by

$$f(\mathbf{r}) = b\left[\left(\frac{r}{a}\right)^2 - 1\right]e^{-(r/a)^2} = \zeta a\left[\left(\frac{r}{a}\right)^2 - 1\right]e^{-(r/a)^2} \quad (1)$$

where $\mathbf{r} = (x, y)$ is a position vector, $r^2 = x^2+y^2$ is the radial distance from the origin, a is the radius of the "event," b is the depth of the "event," and $\zeta = b/a$ is the slope parameter. This shape results in no net seabed mass change, and any sediment "removed" from the center of the pit is "deposited" in a ring around the depression.

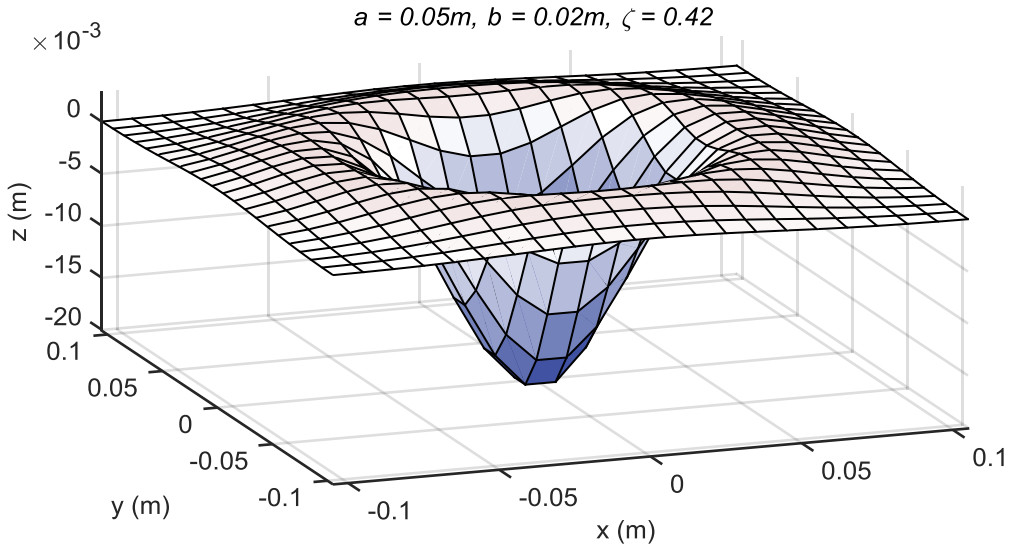

Figure 2: Example bioturbative "event" (note the z-axis exaggeration).

Applying physical insight, the maximum slope this shape may achieve should correspond to the angle of repose (i.e. the slope above which the sediment becomes unstable and immediately collapses), θ_r, of the sediment of interest. Therefore we restrict the slope of the sombrero function model over $0 \le \zeta \le \tan(\theta_r)$

$$0 \le 2\frac{b}{a}\frac{r}{a}\left[2 - \frac{r^2}{a^2}\right]e^{-r^2/a^2} = 2\zeta\frac{r}{a}\left[2 - \frac{r^2}{a^2}\right]e^{-r^2/a^2} \le \tan(\theta_r), \quad (2)$$

and the location of the maximum slope can be found by calculating the inflection points of the 3rd derivative of a Gaussian function. In this notation, the maximum slope occurs at

$$\frac{r^2}{a^2} = \frac{7 - \sqrt{33}}{4}, \quad (3)$$

and combining equations (2) and (3), we have

$$\zeta = \frac{b}{a} \le \frac{\tan(\theta_r)}{1.3803}. \quad (4)$$

3 INCORPORATING HORIZONTAL DIFFUSION

Horizontal diffusion is a widely recognized, albeit poorly quantified, phenomenon impacting seafloor relief. The effect is caused by near-seabed biologic and hydrodynamic activity, combined with the instability of surficial unconsolidated sediment, and results in a continuous "flattening" of the seafloor. The rate of diffusion is spatially and temporally variable, with regions characterized by high biologic

and hydrodynamic activity having seabeds that diffuse or “flatten” faster than barren and stagnant regions. While the mechanisms of horizontal diffusion and quantification of the diffusion rate remain topics of research, diffusion is a phenomenon that can be, and has been, estimated experimentally[1,3] and demonstrated numerically[1,4]. With our model for fish feeding pits in mind, we seek a solution to the diffusion equation

$$\frac{\partial g(\mathbf{r},t)}{\partial t} = D\nabla^2 g(\mathbf{r},t) \tag{5}$$

such that

$$g(\mathbf{r},0) = f(\mathbf{r}). \tag{6}$$

The solution can be found in terms of the Fourier transform

$$G(\mathbf{k},t) = \frac{1}{(2\pi)^2}\int g(\mathbf{r},t)e^{-i\mathbf{k}\cdot\mathbf{r}}d^2r \tag{7}$$

where $\mathbf{k} = (k_x, k_y)$ is a 2-D wave vector. The Fourier transform of equation (5) is

$$\frac{\partial G(\mathbf{k},t)}{\partial t} = -DK^2 G(\mathbf{k},t). \tag{8}$$

The diffusion equation gives

$$G(\mathbf{k},t) = F(\mathbf{k})e^{-Dk^2 t} \tag{9}$$

where $F(\mathbf{k})$ is the Fourier transform of equation (1)

$$F(\mathbf{k}) = \frac{1}{(2\pi)^2}\int f(\mathbf{r})e^{-i\mathbf{k}\cdot\mathbf{r}}d^2r\ , \tag{10}$$

which can be inferred by noting that

$$f(\mathbf{r}) = \frac{4}{a^2}\nabla^2 e^{-r^2/a^2}\ . \tag{11}$$

This suggests that the Fourier transform is of the form

$$F(\mathbf{k}) = Ak^2 e^{-k^2a^2/4}, \tag{12}$$

and can be shown to be true provided

$$A = -\frac{a^4}{16\pi}. \tag{13}$$

The Fourier transform of the sought-after diffusive solution to equation (1) is then

$$G(\mathbf{k},t) = -\frac{a^4}{16\pi}k^2 e^{-k^2a^2/4-Dk^2t}\ . \tag{14}$$

Taking the inverse Fourier transform and rewriting, we now have an equation for a diffusive, inverted, sombrero function (Figure 3)

$$g(\mathbf{r},t) = b\frac{a^4}{\tilde{a}^4}\left[\left(\frac{r}{\tilde{a}}\right)^2 - 1\right]e^{-(r/\tilde{a})^2} = \zeta\frac{a^5}{\tilde{a}^4}\left[\left(\frac{r}{\tilde{a}}\right)^2 - 1\right]e^{-(r/\tilde{a})^2} \tag{15}$$

where

$$\tilde{a}^2 = a^2 + 4Dt\ . \tag{16}$$

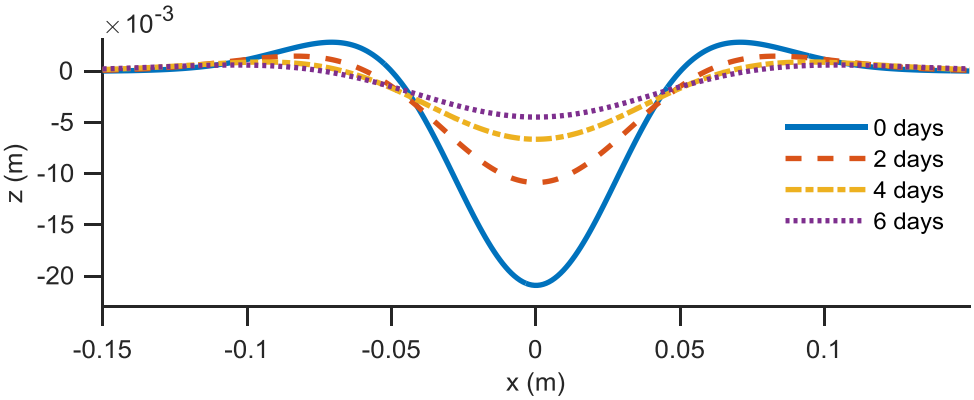

Figure 3: Example profile of bioturbative "event" evolution with D = 1.4e-9 m²/s (note the *z*-axis exaggeration).

4 NUMERIC SIMULATION OF RELIEF AND EVOLUTION

Numeric simulations of seafloor relief may be beneficial for a variety of applications, ranging from oceanographic studies (e.g. hydrodynamic flow in the presence of sand ripples[5]) to prediction of acoustic system performance (e.g. synthetic aperture sonar-based coherent change detection[4]). In this section we will discuss implementation of the previous sections to generate realizations useful for such purposes, and in subsequent sections compare the roughness spectrum generated by numeric simulations to analytic expressions as a measure of veridical realism.

To produce realistic representations of any naturally occurring phenomena, it is generally necessary to incorporate stochastic methods. This is particularly true when the underlying model is deterministic, such as our inverted sombrero function, in order to break up what would otherwise appear too regular[6]. The choice of stochastic models should be tied to our best understanding of physics and biology and supported by experimental observations. In lieu of complete understanding, adopting representative models will often suffice, and when feasible, choosing models which are analytically tractable is often of great benefit.

For the purposes here, we will model the location of bioturbative events uniformly across the simulation area, although it would be possible to introduce a cost function such that events have a higher probability of occurrence in certain regions (e.g. mimic a greater density of "food" in one area making it more likely that a fish feeding pit would occur there). Similarly, while here we will model the rate of deposition of pits as constant with respect to time, this can easily be modified to mimic a diurnal feeding pattern[7].

For the slope parameter random variable, ζ_n, we assume draws from a Beta distribution, a well-known and widely-used distribution[8]. The probability density function of the Beta distribution is

$$p(\mathrm{x}) = \frac{x^{\alpha-1}(1-x)^{\beta-1}}{B(\alpha,\beta)} \tag{17}$$

where α and β are shape parameters, $B(\alpha, \beta)$ is the Beta function (or Euler integral of the first kind), and is defined over $0 \le x \le 1$ which we then scale for purposes here by the maximum slope ($\tan(\theta_t)$ /1.3803) obtained by equation (4).

The Beta distribution has several unique properties that make it an appealing model for the distribution of pit slopes (Figure 4). The two shape parameters, α and β, control the nature of the probability density function (PDF) at the upper and lower bounds respectively. When the shape parameters are equal the PDF is symmetric, and when they are not equal the PDF can be either mildly or strongly skewed. When the shape parameters are equal to 1 the PDF assumes the form of a normal

distribution, and when they are ≥ 2 the probability at the bounds of the distribution approaches zero. Again invoking physical intuition, we expect that both shape parameters will always be ≥ 2 so that the probably of a zero slope and a slope exceeding the angle of repose are both zero, without sacrificing the ability of this model to fit a wide range of experimentally collected data.

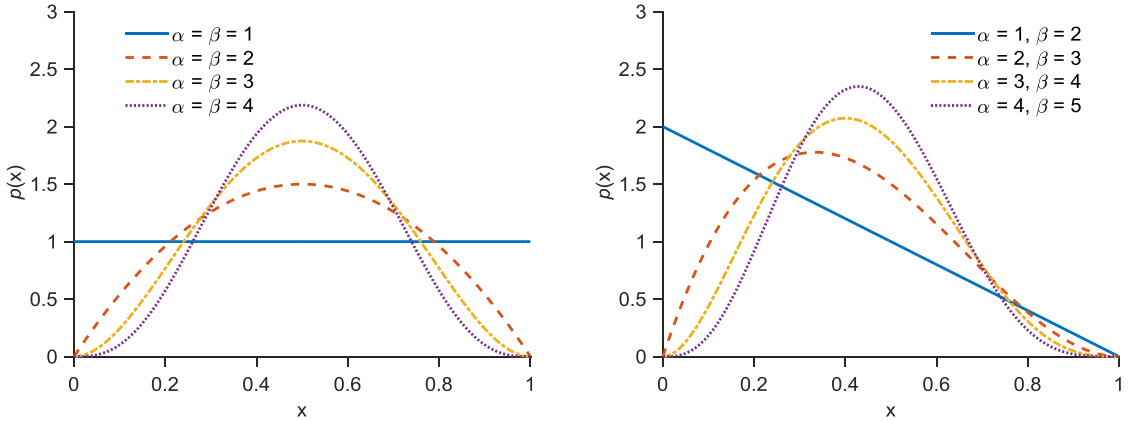

Figure 4: Example Beta-distribution parameters resulting in symmetric (left) and skewed PDFs (right).

The final remaining parameter, pit radius, will be modelled with a variety of distributions as a study to intuit the dependence of equilibrium roughness spectra on the forcing function. For our study here, we consider three distributions which have support over [0,∞), and have one or two parameters: exponential, Rayleigh, and Gamma. The exponential distribution with the static (i.e. non-diffusive) inverted-sombrero function has been shown to lead to a roughness spectrum that is power-law-like[2], and physical intuition supports this choice as these relief functions may be caused by a wide range of biologics (e.g. from small fish to large rays), resulting in a wide range of event sizes. However, it may be unlikely that all scales of events occur in all areas, as this assumed distribution would require. Additionally, the exponential distribution has a high probability of small events (which result in little net change of the relief) but require the same amount of computation as larger events (which result in a larger net change of the relief). The Rayleigh distribution is proposed to be a simplistic model for a single species, while the gamma distribution (with two parameters) allows for greater adjustment of the shape and therefore more flexibility to fit collected data, and is included here as a demonstration. Certainly other distributions can be proposed and used for these simulations, and ideally experimental data could be substituted for any of the stochastic models used here.

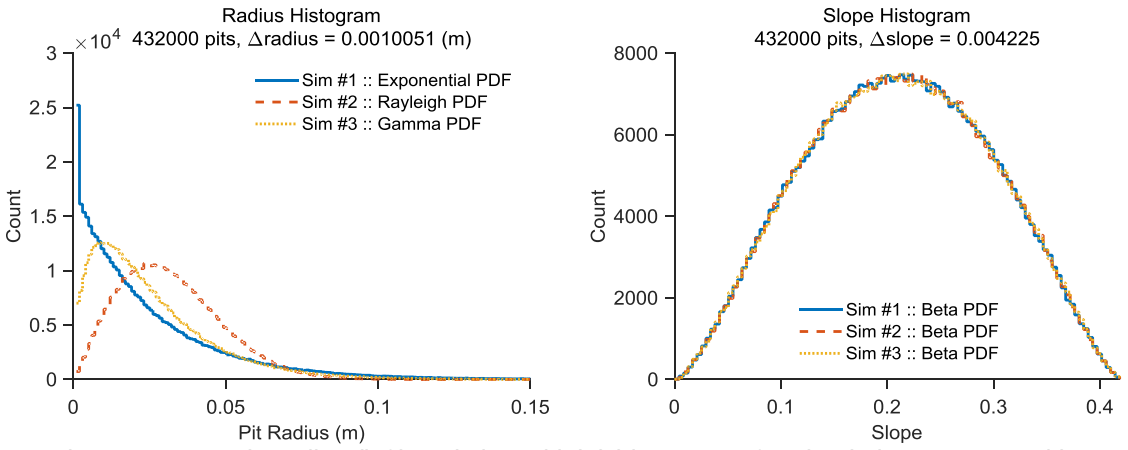

Figure 5: Example radius (left) and slope (right) histograms for simulations presented here.

Example histograms for the radius and slope random variables for the simulations presented here are shown in Figure 5. Example realizations of a surface evolution with the Rayleigh-distributed pit radius are shown in Figure 6 for two time points: one well before equilibrium at t = 1.5 days, and one

approaching equilibrium at t = 50.0 days. Figure 7 shows two example surfaces with differing pit radius distribution models: exponential and gamma. Note the enhanced low-frequency content of the realization generated with the exponential distribution model for radius, as compared to both the gamma- and Rayleigh- (right panel of Figure 6) distributed examples, for the scale and shape parameters used here. For these examples the pit deposition rate (N/TL^2) was 1e-3 pits/s/m^2 and the diffusion constant (D) was 1.4e-9 m^2/s.

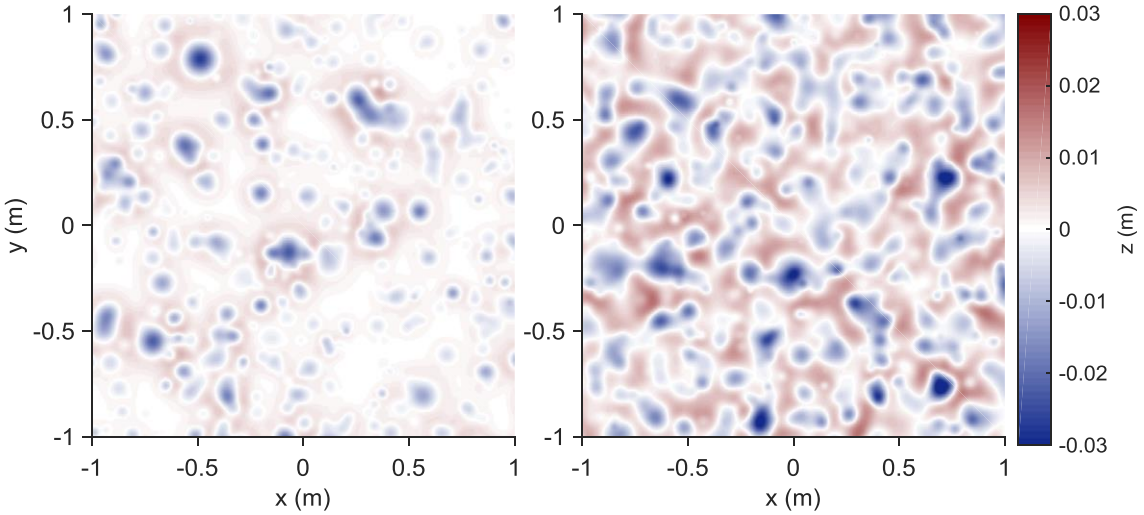

Figure 6: Example surface relief evolution snapshots after 1.5 days (left), and at 50 days (right) with Rayleigh-distributed pit radius and other parameters given in text.

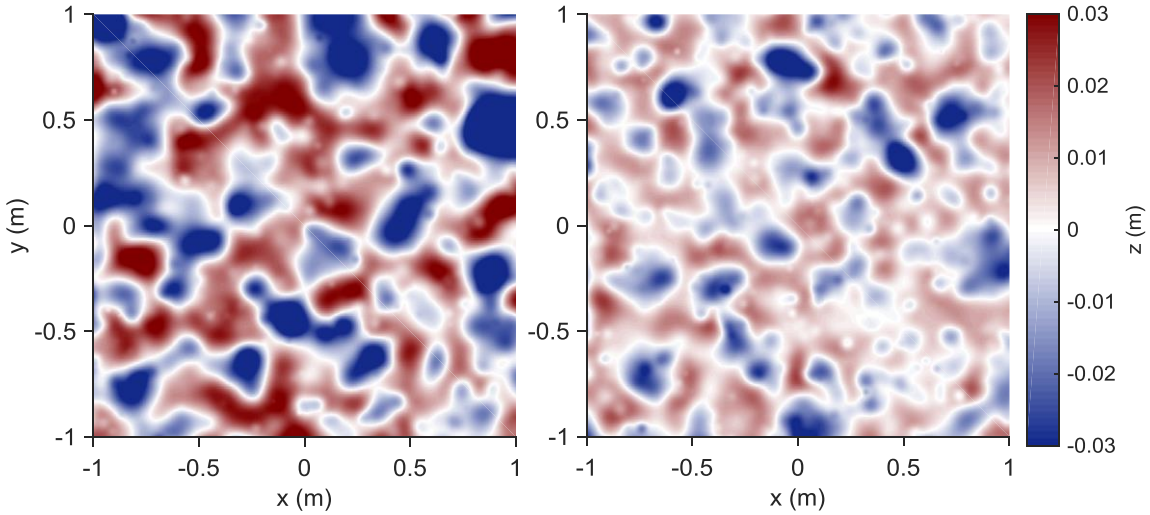

Figure 7: Example surface relief realizations after 50 days for exponential- (left) and gamma- (right) distributed pit radius. Note the increased low frequency content for the exponential distribution model.

5 ESTIMATING EQUILIBRIUM ROUGHNESS SPECTRA

While numerical simulations are beneficial for creating realizations or studying models that are not well-defined analytically, the choice of models presented here allows for concise calculation. In this section we develop an analytic solution to estimate the equilibrium roughness spectra for our bioturbative event model.

Consider a continuous process of adding bioturbative relief functions (such as the inverted sombrero) to existing relief, with the placement and size of each pit chosen randomly. After placement, each pit will begin to degrade (i.e. flatten) owing to diffusion. If this process is continued long enough for the largest pits to degrade, equilibrium will be established and the roughness spectrum will be constant. Consider the Fourier transform of the net relief at time $t = 0$

$$F(\mathbf{k}) = \sum_n b_n G(\mathbf{k}, -t_n, a_n) e^{-i\mathbf{k}\cdot\mathbf{r}_n} . \tag{18}$$

Here, $G(\mathbf{k},t,a)$ is the Fourier transform of a bioturbative relief function that has decayed for time t and has radius determined by parameter a. The times t_n in equation (18) are the times of placement of the n^{th} pit and are all negative. The n^{th} pit is placed at the random position r_n and has amplitude determined by the parameter b_n (or in our case here $\zeta_n a_n$ since we are considering the slope of the pit).

The spectrum will be found by using[1]

$$\left\langle F(\mathbf{k}_2) F^*(\mathbf{k}_1) \right\rangle = W(\mathbf{k}_1)\delta(\mathbf{k}_2 - \mathbf{k}_1) . \tag{19}$$

In forming the expected value in equation (19), all random variables a_n, b_n (or ζ_n), and r_n will be taken to be independent, and cross terms in the double sum implied by equations (18) and (19) will be ignored, as

$$\left\langle e^{-i\mathbf{k}_2\cdot\mathbf{r}_m} e^{-i\mathbf{k}_1\cdot\mathbf{r}_n} \right\rangle = \left\langle e^{-i\mathbf{k}_2\cdot\mathbf{r}_m} \right\rangle \left\langle e^{-i\mathbf{k}_1\cdot\mathbf{r}_n} \right\rangle = 0, \quad m \neq n . \tag{20}$$

Using the form of equation (19) with the Fourier transform of the net relief (equation (18)) , we have

$$\left\langle F(\mathbf{k}_2) F(\mathbf{k}_1) \right\rangle = N \left\langle b_n^2 \right\rangle \left\langle G(\mathbf{k}_2, -t_n, a_n) G^*(\mathbf{k}_1, -t_n, a_n) \right\rangle \left\langle e^{-i(\mathbf{k}_2 - \mathbf{k}_1)\cdot r_n} \right\rangle . \tag{21}$$

In equation (21), N is the total number of pits added in the time interval $-T > t > 0$, where T is a time interval long enough to ensure complete decay of the largest pits. The pit positions r_n will be assumed to be uniformly distributed over a square region having side length L. The factor $\langle \exp(-i(k_2 - k_1) \bullet r_n) \rangle$ in equation (21) approaches a delta function as L approaches infinity. The weight of this approximate delta function can be found as the integral

$$\iint e^{-i\mathbf{k}\cdot\mathbf{r}} p(\mathbf{r}) d^2r \, d^2k = \frac{(2\pi)^2}{L^2} \tag{22}$$

where $p(\mathbf{r})$ is the 2-D PDF for the positions, equal to $1/L^2$ inside the square and zero outside. Finally, using equation (19), the equilibrium spectrum is

$$W(\mathbf{k}) = N \frac{(2\pi)^2}{L^2} \left\langle b_n^2 \, w(\mathbf{k}, a_n, t_n) \right\rangle , \tag{23}$$

where

$$w(\mathbf{k}, a_n, t_n) \equiv \left| G(\mathbf{k}, -t_n, a_n) \right|^2 . \tag{24}$$

The pit spectrum can be factorized into parts dependent on positon and time

$$w(\mathbf{k}, a_n, t_n) = w(\mathbf{k}, a_n) e^{2Dk^2 t} . \tag{25}$$

The average over random placement times is determined by the integral

$$\frac{1}{T} \int_{-T}^{0} e^{2Dk^2 t_n} dt_n = \frac{1}{2Dk^2 T} \tag{26}$$

where it is assumed that T is sufficiently large that $2Dk^2T >> 1$. The equilibrium spectrum can be written as

$$W(\mathbf{k}) = N \left\langle \zeta_n^2 \right\rangle \frac{2\pi^2}{TL^2 Dk^2} \int_0^\infty p(a_n) a_n^2 w(\mathbf{k}, a_n) da_n \tag{27}$$

where $p(a_n)$ is the PDF for the size parameter.

Equation (27) can be interpreted in terms of a simulation as described in the previous section. Over a time interval T, pits are placed randomly in time and space over an area L^2, with each pit having a

size parameter chosen randomly according to the PDF $p(a_n)$. In the early stages, the simulated relief will show growth of roughness; in later stages, it will show random variations of equilibrium roughness.

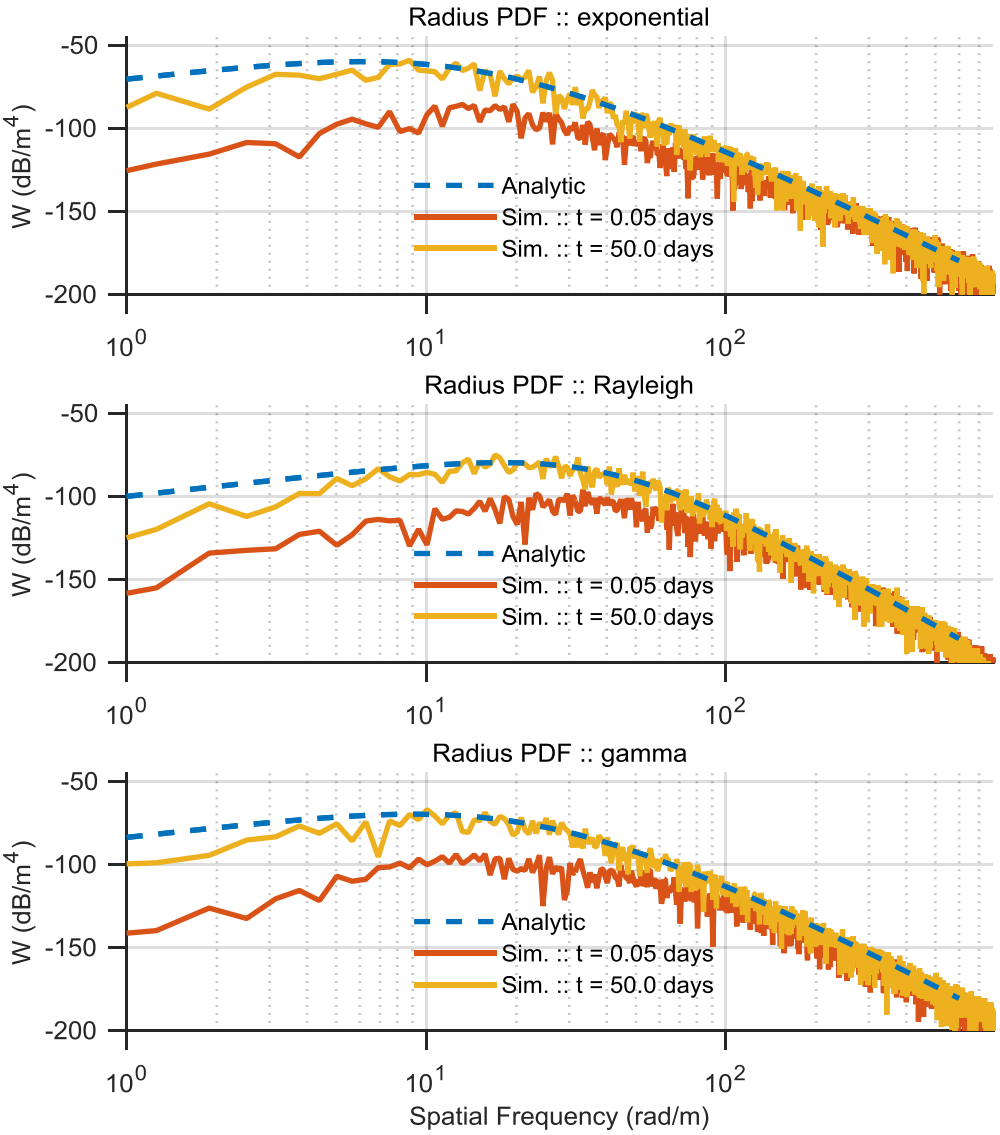

Figure 8: Realization roughness spectra at two time points (t = 0.05 and 50.0 days) for each of the radius distribution models presented here, compared to the analytic expression for equilibrium roughness spectrum.

Returning to the diffusive inverted sombrero function developed earlier, from equations (14), (24), and (25)

$$w(\mathbf{k},a_n) = \frac{1}{\pi^2}\frac{a^8}{256}k^4 e^{-k^2a^2/2}. \tag{28}$$

Then

$$W(\mathbf{k}) = \frac{N\langle\zeta_n^2\rangle}{128TL^2D}k^2\int_0^\infty p(a_n)a_n^{10}e^{-k^2a^2/2}\,da_n. \tag{29}$$

The choice of Beta-distributed slopes makes the evaluation of $\langle\zeta_n^2\rangle$ possible analytically. The Beta distribution moment equation is[9]

$$m_k = c^k \frac{B(\alpha + k, \beta)}{B(\alpha, \beta)} \tag{30}$$

where k is the k^{th} moment, and c is a scaling-constant (for our purposes here $c = \tan(\theta_r)/1.3803$). Combining equations (4) and (30), we have an analytic expression for $\langle \zeta_n^2 \rangle$

$$\left\langle \zeta_n^2 \right\rangle \approx \frac{\tan^2(\theta_r)}{1.3803^2} \frac{B(\alpha + 2, \beta)}{B(\alpha, \beta)}. \tag{31}$$

Combining equations (29) and (31) with knowledge of the pit radius PDF and deposition rate, we are able to estimate the equilibrium roughness spectrum.

6 COMPARISON AND CONCLUSIONS

As the area, number of simulated bioturbative events, and elapsed time grow sufficiently large in the numerical simulation, the roughness spectrum of the realization should approach the equilibrium spectrum given by equation (29). Figure 8 shows the equilibrium roughness spectrum model along with the result of several numerical simulations for each of the three assumed models for the radius distribution.

The agreement between theory and simulation, along with the realism of the surfaces presented previously, demonstrate the efficacy of both the analytic and numerical simulation approaches presented here. However despite these results, a great deal remains to be investigated. Here we have assumed a simplistic model for a bioturbative event (albeit with convenient mathematical properties) as a surrogate for what undoubtedly is a much more complicated shape. The models for the random variables, while based on physical intuition, certainly do not capture all of the insight one might be able to include with knowledge of species and behavior (e.g. organism size distributions, diurnal or seasonal feeding patterns). Finally, a better understanding of the horizontal diffusion phenomenon is needed in order to eventually turn what is currently a measured parameter into a predictable parameter.

7 ACKNOWLEDGEMENTS

The authors appreciate the many useful conversations with colleagues, specifically: DJ Tang (APL-UW), Tony Lyons, (UNH), Doug Abraham (CausaSci), Bruce Newhall (JHU/APL), Brett Bissinger, Derek Olson, and Dan Brown (all of ARL/PSU). This work was supported by the U.S. Office of Naval Research under grants N00014-13-1-0019 and N00014-14-1-0539.

8 REFERENCES

1. D.R. Jackson, M.D. Richardson, K.L. Williams, A.P. Lyons, C.D. Jones, K.B. Briggs, and D. Tang, 'Acoustic observation of the time dependence of the roughness of sandy seafloors,' IEEE J.Ocean.Engr., 34(4) 407-422. (2009).
2. D. Tang, 'Fine-scale measurements of sediment roughness and subbottom variability,' IEEE J.Ocean.Engr., 29(4) 929-939. (2004).
3. A.P. Lyons and D.C. Brown, 'Temporal variability of seafloor roughness and its impact on coherent change detection,' Proceedings of the Institute of Acoustics International Conference on Synthetic Aperture RADAR and SONAR, Lerici, Italy. (2010).
4. S.F. Johnson and A.P. Lyons, 'Simulation of rippled-sand seafloor evolution for synthetic SAS imagery,' Proceedings of the 4th Underwater Acoustic Measurements Conference: Technologies and Results, Kos, Greece. (2011).
5. A. Penko, S.F. Johnson, and J. Calantoni, 'Simulation of measured seafloor roughness spectrum time series using a coupled ripple-bioturbation model,' Proceedings of the Institute

of Acoustics Seabed and Sediment Acoustics: Measurements and Modelling, Bath, United Kingdom. (2015).

6. D.S. Ebert, F.K. Musgrave, D. Peachy, K. Perlin, and S. Worley, Texturing and Modeling: A Procedural Approach, 3rd ed, Morgan Kaufmann. (2003).
7. K. Kringel, P.A. Jumars, and D.V. Holliday, 'A shallow scattering layer: high-resolution acoustic analysis of nocturnal vertical migration from the seabed,' Limnol.Oceanogr., 48, 1223-1234. (2003).
8. N.L. Johnson and S. Kotz, Continuous Univariate Distributions – 2, Houghton Mifflin. (1970).
9. M. Fisz, Probability Theory and Mathematical Statistics, 3rd ed, Krieger. (1963).